CrossMark

ORIGINAL ARTICLE

Liquefaction record of the great 1934 earthquake predecessors from the north Bihar alluvial plains of India

C. P. Rajendran · Biju John · Kusala Rajendran · Jaishri Sanwal

Abstract The great 1934 Himalayan earthquake of moment magnitude (Mw) 8.1 generated a large zone of ground failure and liquefaction in north Bihar, India, in addition to the earthquakes of 1833 (Mw ~7.7) and 1988 (Mw 6.7) that have also impacted this region. Here, we present the results of paleoliquefaction investigations from four sites in the plains of north Bihar and one in eastern Uttar Pradesh. The liquefaction features generated by successive earthquakes were dated at AD 829–971, 886–1090, 907–1181, 1130–1376, 1112–1572, 1492–1672, 1733–1839, and 1814–1854. One of the liquefaction events dated at AD 829–971, 886–1090, and 907–1181 may correlate with the great earthquake of AD ~1100, recognized in an earlier study from the sections across the frontal thrust in central eastern Nepal. Two late medieval liquefaction episodes of AD 1130–1376 and 1492–1672 were also exposed in our sites. The sedimentary sections also revealed sandblows that can be attributed to the 1833 earthquake, a lesser magnitude event compared to the 1934. Liquefactions triggered by the 1934 and 1988 earthquakes were evident within the topmost level in some sections. The available data lead us to conjecture that a series of temporally close spaced earthquakes of both strong and large types, not including the infrequent great earthquakes like the 1934, have affected the Bihar Plains during the last 1500 years with a combined recurrence interval of 124 ± 63 years.

Keywords Liquefaction · 1934 Bihar-Nepal earthquake · Earthquake recurrence · Bihar Plains

1 Introduction

Tectonic models suggest that the great Himalayan earthquakes of moment magnitude (Mw) >8.0 originate on a décollement, called the Main Himalayan Thrust (MHT), and their ruptures propagate southward to the Himalayan frontal thrust (HFT) whereas large and moderate earthquakes occur on the blind crustal ramps (Fig. 1a, b), which may coincide with the duplex zone south of main central thrust (MCT; Seeber and Armbruster 1981; Pandey et al. 1995). The southward propagating ruptures from great earthquakes may cause significant damage and ground deformation in the Indo-Gangetic plains, as exemplified by the 1934 Nepal-Bihar (Mw 8.1) earthquake of January 15, 1934. The epicenter of this earthquake is located 10 km south of Mt. Everest (Chen and Molnar 1977; Fig. 1a). Apart from the meisoseismal area in Nepal, the 1934 earthquake impacted the north Bihar alluvial plains of India bordering Nepal and generated extensive lateral spreading and

C. P. Rajendran (✉) · J. Sanwal
Geodynamics Unit, Jawaharlal Nehru Centre for Advanced Scientific Research, Bangalore 560064, India
e-mail: cprajendran@gmail.com

B. John
National Institute of Rock Mechanics, Kolar Gold Fields 563117, India

K. Rajendran
Centre for Earth Sciences, Indian Institute of Science, Bangalore 560012, India
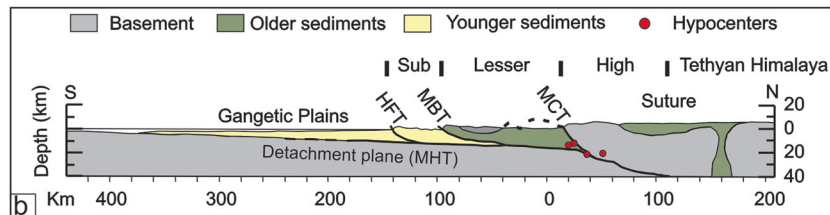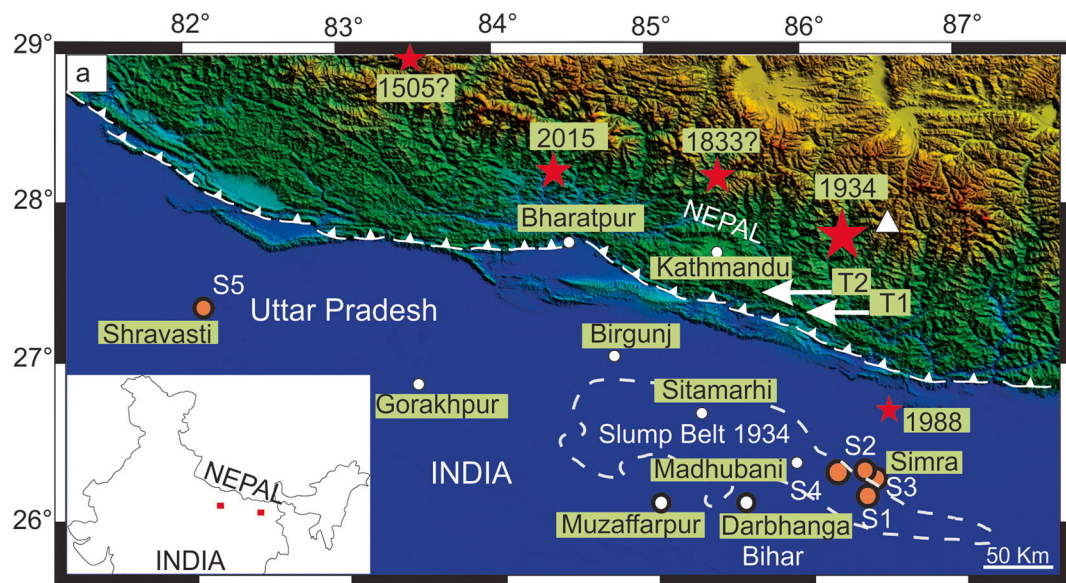
Fig. 1 a The tectonic map of Himalaya showing the epicentral locations of the Mw 8.1, 1934 (Chen and Molnar 1977) and Mw 6.7, 1988 earthquakes (Nandy et al. 1993) along with approximate locations of the 1505 (Ambraseys and Jackson 2003; Ambraseys and Douglas 2004) and the Mw ≤7.7, 1833 earthquakes (Bilham 1995). Location of the April 25, 2015 Mw 7.8 Nepal earthquake is also shown. *T1* and *T2* denote trench sites of Lavé et al. (2005) and Sapkota et al. (2013) on the Himalayan Frontal Thrust from where evidence of AD 1100 and 1255 earthquakes were obtained, respectively, and *white triangle* marks Mt. Everest. Liquefaction study sites are marked as *S1*, *S2*, *S3*, *S4*, and *S5*. The 1934 slump belt is outlined by *dotted line*, and the *white discontinuous* *line with teeth* denotes the Himalayan Frontal Thrust. *Inset*: map of India-Nepal showing study area (*filled red squares*); b Generalized cross section of the central Himalaya showing the main central thrust (MCT), main boundary thrust (MBT), Himalayan frontal thrust (HFT), and the main Himalayan thrust (MHT) (Seeber and Armbruster 1981). *Solid red circles* underneath the MCT indicate the source zone of Himalayan earthquakes. **c.** Photograph showing sandblows (1, 2, and 3) at site S2 in Simra Village, Bihar, associated with the 1988 earthquake (after Nandy et al. 1993; see text for further discussion). **d** Photograph of a filled sandblow crater taken in 2012 at the location shown in **c**

liquefaction (Dunn et al. 1939). The most affected areas include the towns of Sitamarhi, Madhubani, and Darbhanga in Bihar, and the region also subsided, forming a "slump belt" (Fig. 1a). This led some workers to suggest that downfaulting took place under the alluvial plains (Seeber and Armbruster 1981). This perception was also augmented by the early reports of the damage associated with this earthquake, especially the one compiled by Dunn et al. (1939), which was skewed towards north Bihar. The non-availability of equally representative damage reports from Nepal at that time compounded by seismic wave amplification and extensive damage within the Bihar Plains possibly led to the initial fixing of its epicenter about 200 km south of the actual location (Dunn et al. 1939). A zone of equally severe damage (IX and X on the Rossi-Forel scale), that included both ground failure and soil liquefaction, was recognized in the central eastern Nepal extending into the Kathmandu Valley to the west (Pandey and Molnar 1988; Rana 2013). Using the relocated epicenter (~10 km south of Mt. Everest at 27.55° N, 87.09° E) and the region of maximum shaking intensity and subsidence as proxy measures of the centroid, Bilham (1995) suggests that the rupture propagated from east to west for a distance of about 160 km. Apart from the rupture directivity, the exceptionally wide zone of liquefaction in the Bihar Plains is now attributed mainly to high ground motions caused by basin resonance (Hough and Bilham 2008).

Another destructive earthquake occurred in the region in 1833, with a moment magnitude of ~7.7, estimated on the basis of felt reports (Bilham 1995). Although the 1833 and 1934 earthquakes show somewhat overlapping intensity patterns, contemporary reports do not mention any conspicuous liquefaction field for the former (Bilham 1995). Subsequently, paleoliquefaction investigations in the region, however, reported a moderate distribution of liquefaction attributable to the 1833 earthquake (Sukhija et al. 2002). Although unconnected to Himalayan thrust tectonics and sourced under the Nepal Plains, this region was again impacted during a strong deep crustal earthquake (Mw 6.7) in 1988 (Fig. 1a), leading to localized liquefaction (Nandy et al. 1993; Ghimire and Minoru 2007). The shorter epicentral distance (~50 km), rather than its magnitude, must have been one factor that favored liquefaction in the region, but the fact that the site liquefied despite the lower crustal source suggests its high liquefaction susceptibility.

Recent trenching excavations have identified surface rupture associated with the 1934 earthquake along the main frontal thrust of central Nepal (Sapkota et al. 2013; Fig. 1a for locations of trenches T1 and T2). Paleoseismic evidence from the same site suggests another great earthquake and was suggested to be correlative of the historically reported AD 1255 earthquake (see Fig. 1a for the trench site T2). Lavé et al. (2005) recorded stratigraphic offsets from an adjacent area, from a great earthquake that occurred around AD 1100 (Fig. 1a for location of the trench site T1). These events, if they were from the same source zones, are expected to generate equally intense and overlapping liquefaction fields in the alluvial plains of north Bihar and eastern Uttar Pradesh. With such closely spaced great earthquakes (AD 1100 and 1255), it is difficult to identify which of these events is the true predecessor that has affected the source zone of the 1934 earthquake. Another scenario is that the AD 1100 and 1255 earthquakes belong to adjacent segments that ruptured in opposite directions and overlapped at the extremity of their respective segments (Rajendran et al. 2015). In fact, the case of the April 2015 Nepal earthquake that ruptured ~150 km eastward from its source (as compared to westward directivity of the 1934 earthquake) demonstrates not only the existence of multiple sources but also the variable rupture directivity of Himalayan earthquakes (Parameswaran et al. 2015).

Tibetan archival information suggests that a damaging earthquake occurred in the region in AD 1505, and some workers consider this as a great earthquake (e.g., Ambraseys and Jackson 2003). The source of this earthquake is reported to be close to Mustang on the Nepal-Tibert border (Fig. 1a). If the moment magnitude of the 1505 earthquake is >8, then it is expected to propagate across the Himalaya through the MHT to rupture at the HFT and produce a large liquefaction field in the Gangetic Plains, west of the 1934 slump belt (Fig. 1a). Rupture characteristics and source zone of the 1505 earthquake are less certain and questions have been raised regarding its size (Rajendran et al. 2013). It is possible that the 1505 earthquake was of lesser magnitude that affected some Tibetan monasteries but did not impact the Gangetic plains by generating a large liquefaction field or causing any damage, which would probably explain why no historical references to this earthquake are available from the Indian side or even from Nepal where the impact should have been equally intense (Rajendran and Rajendran 2005; Rajendran et al.

2013). The historical information from Nepal, on the contrary, indicates a destructive earthquake in the year 1681 (Rana 2013). It is also worth noting that the recent April 25 Nepal earthquake (Mw 7.8), comparable in size to that of the 1833 earthquake, did generate minimal liquefaction in the Madhubani District of north Bihar, according to a report by the Geological Survey of India (http://www.portal.gsi.gov.in/gsiDoc/pub/nepaleq_%20liq.pdf). A zone of liquefaction spreading intermittently over 3 km expressed as sinuous ground fissures through which sand and water rose to a height of 1 m had been identified here. Some of these sites are reported to have been reactivated in a smaller scale (3–5-cm-wide 'blister' like sandblows) just after the 12 May 2015 aftershock (Mw 7.3), as well.

Ambiguity of historical records and incompleteness of paleoseismic data have created difficulties in assessing the pattern of earthquake recurrence on the 1934 segment. As seismically induced liquefaction features serve as useful proxies of past major earthquakes, they offer an alternate way to constrain the recurrence period of major earthquakes if their timings can be constrained. As exemplified by the 1934 event, the great earthquakes originating on the MHT are believed to emerge at the HFT and impact the Gangetic plains. Therefore, the northern Bihar alluvial plains located adjacent to the interface of the HFT offer an ideal setting to understand the behavior of the Himalayan thrusts by studying the pattern and extend of liquefaction fields produced by respective earthquakes. Here, we present the results from a pilot field study and report the age constraints of the liquefaction features identified in the region.

2 Background and research approach

Liquefaction is the transformation of saturated cohesionless granular material from solid to liquefied state due to increased pore-pressure triggered by earthquake-induced shear stresses (Housner 1958). The water expelled from the underlying liquefied sand due to shaking accumulates beneath a low-permeability capping layer to form a water-rich zone, and it is from here that much of the water and sand that vents to the surface after explosively breaking the cap (Fig. 2a, b). While the process of earthquake-induced liquefaction and its impact on built structures has been a primary focus from the point of view of earthquake engineering (Youd 1973; Seed 1979), the importance of these features in determining earthquake histories was recognized soon after the 1971 San Fernando, California, earthquake (Sims 1973). Since then, liquefaction features or what may be termed as sandblows have been used as proxies to determine seismic history in various geological and tectonic settings (e.g., Russ 1979; Obermeier et al. 1985; Talwani and Cox 1985; Tuttle and Seeber 1991; Rajendran and Talwani 1993; Sims and Garvin 1995; Rajendran and Rajendran 2001; Tuttle et al. 2005; Tuttle et al. 2006).

The approach to elucidating seismic history primarily involves identifying and characterizing liquefaction features and constraining their relative ages. Identifying different generations of multiple features requires deciphering the crosscutting relationships between the sedimentary structures or features and their order of superposition. The relative ages of these structures/features are determined using both radiocarbon dating of the embedded organic material and optically stimulated luminescence dating of the sandy layers. Upper (maximum) and lower (minimum) or contemporaneous ages of the liquefaction feature in question can be determined by dating different parts of the section, as shown in Fig. 2b. Global examples show that multiple earthquakes occurring at different time intervals are commonly represented by recurring liquefaction in a given site that mostly exploits the same dike for venting (Youd 1984; Saucier 1989; Tuttle and Seeber 1991; Obermeier 1994; Obermeier et al. 1995; Sims and Garvin 1995).

The study sites in northern Bihar were selected based on the historical accounts and reports of the liquefaction during the 1934 earthquake. Reports of the 1988 earthquake (Mw 6.7) that described liquefaction, especially in Darbhanga area, were also a consideration for the choice of study sites (Fig. 1c, d). Thus, the availability of extensive field reports of the two earthquakes has aided our exploration to locate potential sites for paleoliquefaction studies. As a prelude to locating the trenches, we recorded the depth to water table and the stratigraphic superposition of various lithologies in the selected study sites. Trenches (5–10-m long and 2–4-m deep) were excavated in such sites, after ascertaining the depth to the local water table and local shallow stratigraphy. We used standard criteria that include presence of rip-up clasts within the vents, nature of internal bedding (fining upward sequences), and structures indicating
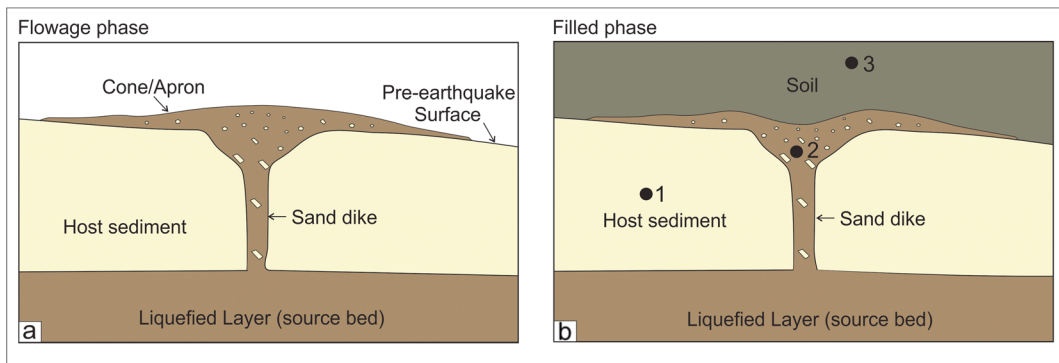
Fig. 2 Schematic cross section of a sandblow in different stages of its formation and preservation showing various parts of its structure and terminology used in the text: **a** Coseismic stage marked by upward directed flow of sediment-water mix cutting across the pre-earthquake surface. **b** Post-seismic stage showing discharged material has partly flowed back or collapsed into the crater, later buried by re-sedimentation processes and development of a new soil profile. *Black circles* 1, 2, and 3 represent maximum, contemporary, and minimum ages of the sandblow

water escape and fluidization (load casts and convolute lamination) to distinguish the seismically induced liquefaction and sandblows from the regular layers.

Different generations of seismically induced paleoliquefaction features or sandblows (dikes, sills, sand vents, and cones) were identified based on their crosscutting relationships or from the beds representing the periods of intereseismic deposition that separate the event layers. However, one caveat is that the geological sections may not necessarily expose the center of the sandblow in many occasions, and therefore, what finally get revealed in the cross sections would probably not represent the feature in its entirety (as shown in Fig. 2a). Such sections might show parts of the features such as sills, dikes, vented sediments (in the form of cones or sand aprons) and different types of soft sediment deformations. The out-of-sequence sandy beds, if they are indeed products of liquefaction, would generally be associated with feeder dikes or contain clasts of host sediments within them suggesting strong upward directed hydraulic force. The discordant beds of liquefaction origin within a sedimentary section can be considered as products of discrete events, separated in time, and the dates obtained on them may reveal their temporal distinctiveness from that of the host sediment. Additional criteria can be obtained from the known local historical earthquakes that provide calibration cues for the events that occurred further back in the past. Following these methods, we identified different generations of liquefaction features from trench sections. Samples for age determination were collected from different stratigraphic levels, to obtain maximum, minimum, and contemporaneous ages. We obtained accelerator mass spectroscopy (AMS) dates for the organic materials, and in the absence of organic material, we relied on optically stimulated luminescence (OSL) dating techniques to determine the ages of the samples (Tables 1 and 2).

3 Field investigations and results

As discussed earlier, the reports on the 1934 earthquake describe areal extent of coseismic ground failure and liquefaction in Madhubani and Darbhanga Districts of the Bihar Province (Dunn et al. 1939) that form the major part of the slump belt. The sandblows and lateral spreads generated during the 1988 earthquake are also concentrated between Darbhanga in Bihar and India-Nepal border (Nandy et al. 1993). Following the leads mentioned in the reports of these earthquakes, we located the sites of 1988 liquefaction near Simra and Paiharpur Villages within the slump belt, and four of our trenches were dug across at these sites. An outlying site was independently selected near the town of Shravasti, located about 250 km west of the slump belt (Fig. 1a).

3.1 Site 1

The site S1 in the village of Simra (N 26° 16′ 14.9″; E 86° 18′ 3.7″) revealed a 1.67-m deep sedimentary section consisting of alternating brownish silty clay and white sandy layers (Fig. 3a, b). The top part (~35 cm)

Table 1 Data on radiocarbon dates of the charcoal/wood fragments from the liquefaction sites

Sample ID/site no.	^{14}C age	1 sigma	2 sigma
SIM-1/L1/1 NZA 40185 (site 1)	1201 ± 20	AD 774–868	AD 770–886
SIM-1/L1/2 NZA 40154 (site 1)	577 ± 15	AD 1323–1404	AD 1315–1411
SIM-2-L1 BS 3453 (Site 2)	260 ± 20	AD 1642–1661	AD 1528–1796
RAP/SB-2/B/P10 NZA 40186 (site 5)	1006 ± 20	AD 998–1031	AD 988–1116
RAP/W1/P7 BS 3459 (site 5)	2030 ± 80	BC 158–AD 54	BC 352–AD 132

AMS dating of charcoal samples were conducted at Rafter Radiocarbon Laboratory (New Zealand). Radiocarbon ages were calibrated using CALIB version 7.0.2 (Reimer et al. 2013). The two sigma ranges have maximum area under the probability distribution curve

of the section is disturbed due to plowing activity. One conspicuous feature exposed here is a narrow (2-cm wide) tubular feeder dike that gets wider towards the upper level (denoted by "D" in Fig. 3b). The feeder dike typically ends up in a crater like depression (denoted by "C" in Fig. 3b) with an overlying blanket of whitish silty

Table 2 Quartz optically stimulated luminescence (OSL) ages of sediment samples

Lab No.	Sample no./site no.	Sample depth from surface (m)	U (ppm)	Th (ppm)	Potassium K (%)	Moisture content (%)	Equivalent dose (De) Gy	Dose rate (Gy/ka)	Age (years)	Age (AD)
LD1190	SIM-1/SB-1/ site 1	1.0	1.47	4.6	1.20	0.32	2.22 ± 0.14	1.99 ± 0.02	1112 ± 71	829–971
LD1197	SIM-1/SB-2/ site 1	1.25	1.5	12.1	2.18	16.40	0.52 ± 0.06	2.92 ± 0.05	178 ± 20	1814–1862
LD1201	SIM-2/SB-3/ site 2	1.0	0.79	6.8	1.62	1.36	2.42 ± 0.24	2.36 ± 0.04	1024 ± 102	886–1090
LD1191	SIM-2/SB-2/ Site 2	1.50	0.81	13.6	1.80	0.18	2.93 ± 0.42	3.02 ± 0.03	968 ± 137	907–1181
LD1192	SIM-3A/1/site 3	0.30	1	8.3	1.13	0.03	1.57 ± 0.17	2.10 ± 0.02	746 ± 80	1186–1346
LD1193	SIM-3A/2/site 3	0.50	0.41	5.1	1.39	1.93	1.48 ± 0.24	1.95 ± 0.02	759 ± 123	1130–1376
LD 1429	P/T6/OSL-1/ site 4	0.95	4.34	14.9	1.20	1.0	2.21 ± 0.75	3.3 ± 0.2	670 ± 230	1112–1572
LD 1428	P/T6/OSL-2/ site 4	0.50	4.78	19.0	1.35	1.0	1.65 ± 0.33	3.9 ± 0.2	430 ± 90	1492–1672
LD1198	P/T6/OSL-3/ site 4	0.45	1.13	14.6	1.77	6.04	0.67 ± 0.16	2.97 ± 0.04	226 ± 53	1733–1839
LD1196	RAP-1/site-5	1.75	0.69	2.8	0.96	1.21	0.57 ± 0.16	1.43 ± 0.01	399 ± 110	1613–1723
LD 1197	RAP-2/site 5	1.25	1.5	12.1	2.18	16.40	0.52 ± 0.06	2.92 ± 0.05	178 ± 20	1814–1854

Optically stimulated luminescence (OSL) measurement were carried out in an automated Riso TL/DA 15 reader equipped with filtered green light from a halogen lamp, which is located at the Wadia Institute of Himalayan Geology, Dehra Dun, India. The equivalent dose (ED) values were calculated using the initial integral of the OSL by Duller Analyze software. For the annual dose rate estimation, concentration of uranium, thorium, and potassium in the sediments were measured by XRF. The water content was determined for all the samples by heating at 100 °C. The single aliquot regeneration protocol (Murray and Wintle 2000; 2003) was used for equivalent dose determination

sand (denoted by "A" in Fig. 3b) that contains reddish brown clasts. The upper part of the conical crater has two stratified lenses of clay that has filled the depression and has also incorporated a few angular clasts of the host sediment (brownish silty clay). The sandy clay layers probably represent fine-grained sediments deposited during the "waning" phase of sand extrusion. The tubular dike at the middle level of the section cross cuts the aforementioned whitish layer of silty sand (denoted by "A" in Fig. 3b) that has irregular boundaries with the host sediment and is also associated with what appears to be a truncated feeder dike (Fig. 3b). The sandy layer contains a few clasts of the host sediment of brownish silt. The characteristics of this unit thus conform to what could be characterized as an apron: an emplaced sandy bed associated with a sandblow or an intruded sill that is embedded within the host sediment (Obermeier 1994). The feature itself is crosscut by several vertical dikes that feed into the uppermost sandy layer.

Age constraints were developed on the basis of two radiocarbon AMS dates (AD 770–886 and 1315–1411) and one OSL date of AD 829–971 (1112 ± 71 years) (Tables 1 and 2; Fig. 3a, b). Among these dates, the OSL date of AD 829–971 (1112 ± 71 years) denotes the contemporaneous age of the older event (sandblow-1 in Fig. 3a). The radiocarbon date of AD 770–886 obtained at the lower part of the host sediment brackets the maximum age of sandblow-1. A feeder dike occurs just above sandblow-1, and the AMS date of AD 1315–1411 provides the maximum age of the dike (sandblow-2 in Fig. 3a). The OSL date of AD 1814–1862 provides the maximum age for the third generation event (sandblow-3 in Fig. 3a), which probably represents the 1833 earthquake. We recorded several feeder dikes cross cutting the third generation feature that ends up at the lower boundary of the uppermost sandy layer, which is likely to represent the great 1934 earthquake. The top part of the section is highly disturbed by tilling activities and the original sedimentary structures have been destroyed.

3.2 Site 2

The trench at site S2 (N 26° 16′ 50.0″; E 86° 18′ 18.2″; Fig. 1a) was cut in a topographical depression, which is reported to be a filled crater generated during the 1988 earthquake (Fig. 1c, d). The 9-m-long trench exposed a complex picture of successive generations of sediment deformation. The deformation layers (composed of fine

sand) are identified on the southern wall and the eastern wall based on the presence of mud clasts and flow structures (Fig. 3c, d). Incorporation of clasts derived from the host sediment indicates that these features are consistent with an explosive upwelling from a vent (Obermeier et al. 1995). The contact between the original host sediment and crater wall (on the southern wall) is relatively sharp. The suspected deformation layers (1 to 7 in Fig. 3d) are succeeded either by crater-fill sequences or separated by erosional surfaces.

The successive crater-fill sequences between deformed layers might have been formed by rainwater and flooding that also carry the surrounding vented sand. During interseismic periods these may have been transported back into the crater along with other surficial material. These sedimentation wedges separating individual liquefaction layers are representative of the time elapsed between episodic earthquake activities. We could recognize three such events recurring within the same crater. The radiocarbon age of AD 1528–1796 obtained from woody material from the lower part of the crater is assumed here as an upper age limit of sandblow-4 in this crater. The overlapping sandblow formations of 1833, 1934 and 1988 events are also represented here at the upper levels (Fig. 3c, d). The closely spaced events of liquefaction at the site lead to repeated churning of previous deposits within the crater. This results in blurring of contacts between the sedimentary beds, often creating difficulties for isolating individual events from the sedimentary sections (e.g., Saucier 1989); a common problem encountered in the interpretation of what is called a "compound sandblow" (Sims and Garvin 1995).

Three white sandy layers interbedded with clay occur at the lower level of the trench on the eastern side, which show a cross cutting relationship with the crater boundary (Fig. 3c, d). These sandy layers within the clayey host sediment contain mud clasts that are possibly derived from host sediment. The sandy layers may represent part of sandblow cones formed earlier than the present crater. We obtained two OSL dates of AD 886–1090 and 907–1181 from two layers, which are considered as contemporaneous ages of the corresponding sandblows (Table 2).

3.3 Site 3

At site 3 (S3) in Simra (N 26° 16′ 42.8″; E 86° 18′ 28.7″; Fig. 1a), we logged a section adjacent to cultivated land
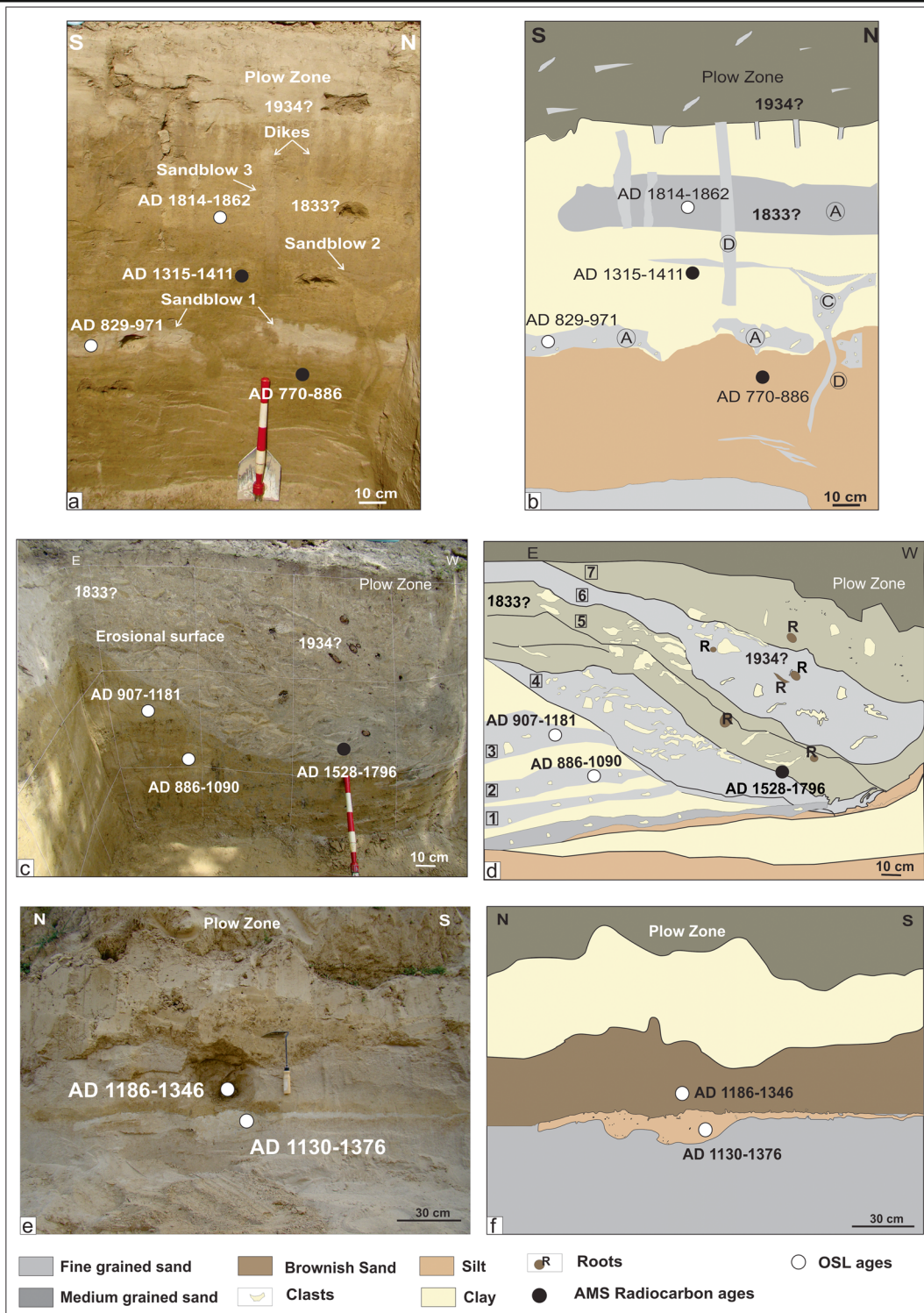
Fig. 3 **a** Section (southern wall) at Site S1 in Simra Village. **b** Sketch highlighting the features (dikes (*D*), craters (*C*), and aprons (*A*) exposed in the section). **c** Section (west wall) at site S2 in Simra Village. **d** Sketch highlighting the features exposed on the section at site 2; liquefaction events from 1 to 7 are also indicated. **e** Section at site S3 in Simra Village. **f** Sketch of the section showing main features. *Black circles*: radiocarbon ages; *white circles*: optically stimulated luminescence dates. See Fig. 1 **a** for locations of these sites

(Fig. 3e). A sand layer, which pinches out laterally, is exposed 1.5 m from the surface between underlying brownish clay and an overlying bed of reddish sand (Fig. 3f). The upper part of the section is either reworked due to agricultural activities or it is a man-made fill material, and the aforesaid sandy layer occurs >1 m below the reworked zone. Upper and lower boundaries of this sandy layer make sharp contacts with the host sediment. Our attempts to trace the feeder dike within the section were not successful, but the unit's characteristics including its irregular outline of the sandy layer (often marked by sandy protrusions of the event layer at the upper contact with the host sediment) convolute laminations and presence of clasts suggest that it could be an emplacement from below and not a product of regular sedimentation. The OSL date AD 1130–1376 from the deformation layer provides the timing of liquefaction episode, and the OSL age AD 1186–1346 obtained from the host sediment overlaps with the age of the event layer.

3.4 Site 4

The site S4 is located in the village of Paiharpur (N 26° 23′ 54.1″; E 86° 07′ 00.1″) about 10 km northwest of sites 1–3 (Fig. 1a). A large number of sandblows caused by the 1988 earthquake are reported from this area. Even today, the sites of 1988 sandblows continue to remain as circular depressions that have become the locales of rainwater pools (Fig. 4a). We made five trenches at this location, and all of the sections revealed repeating white sandy layers alternating with brownish clay (Figs. 4b).

The section presented here exposes three white sandy deformed layers (1, 2, and 3) with variable thickness (20–30 cm). These intervening sandy layers are characterized by convolute laminations and contain clasts of brownish clay (Fig. 4a). The lower contacts of these layers with the black clay show occasional ~2-cm-wide dikes. The dikes form the conduits for the emplacement of white sand from deeper sources. The OSL dates of AD 1112–1572, 1492–1672, and 1733–1839 obtained from the three sandy layers from bottom to top are assumed to be contemporaneous dates of the corresponding liquefaction episodes.

3.5 Site 5

Exposed on the southwestern bank of Rapti River near the town of Shravasti (N 27° 32′ 20.7″; E 82° 02′ 34.9″) in the eastern Uttar Pradesh, the site S5 is a natural section of river alluvium, located ~200 km west of the other four sites (Fig. 1a). The site was chosen primarily because of its accessibility and it displayed an 80-m-long unhindered exposure dominated by alternating layers of cross-bedded and laminar sand, interbedded with clay (Fig. 5; top panel). The four deformation features identified along this section occur at three different levels. The sedimentary beds in which these features occur are marked by erosional contacts with the overlying layers (Fig. 5; A–D).

Morphologically, these features share characteristics of craters containing a homogeneous matrix of sand incorporating clasts composed of clay that are characteristically associated with sandblows (Fig. 5; middle
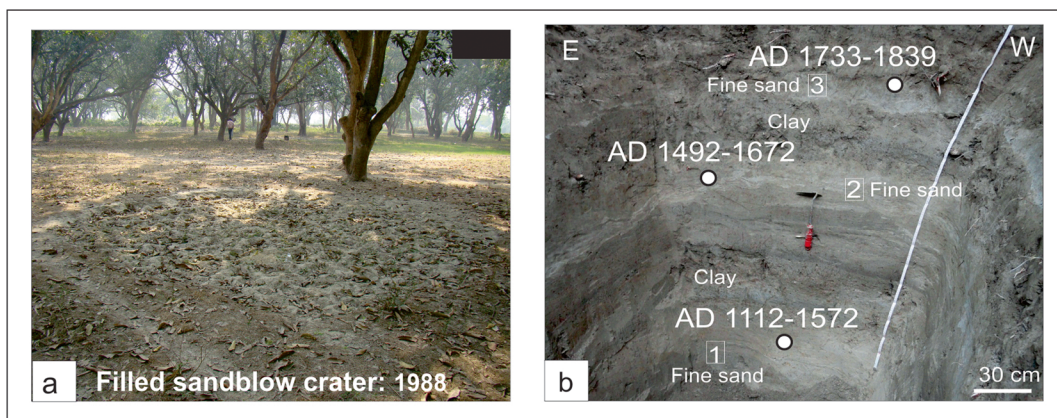

Fig. 4 **a** Trench location (northern wall) at Paiharpur. **b** A photograph of the trench section at Paiharpur (site 4) showing repeating sandblows within the section representing previous liquefaction events (*white circles*: optically stimulated luminescence dates)
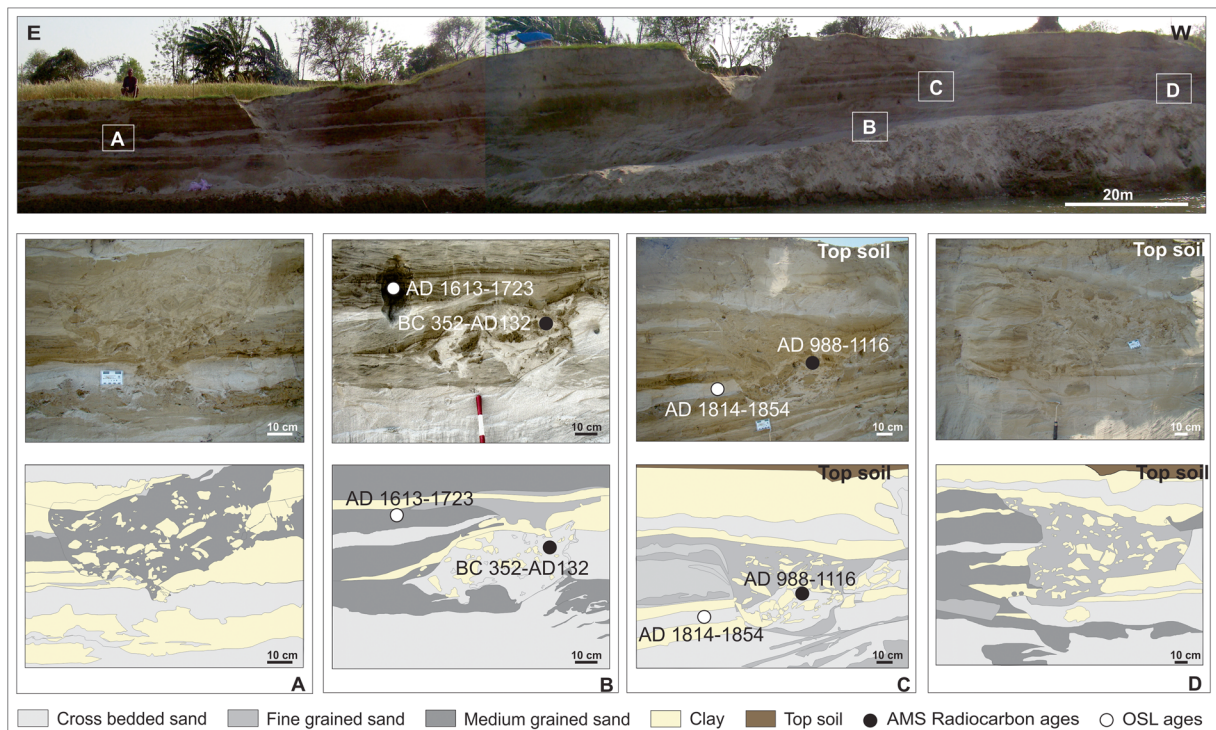
Fig. 5 *Top panel*—section (southern wall) on the bank of Rapti River near the town of Shravasti in the eastern part of the State of Uttar Pradesh: *A*, *B*, *C*, and *D*. *Middle panel*: liquefaction features observed on the section. *Bottom panel*: corresponding sketches of the features shown in middle panel

and bottom panels). The occasional association with feeder dikes further implies that these craters could be "pop-up" structures formed by liquefaction that breaks the continuity of horizontally laid beds (Fig. 5; A–D in middle and lower panels). While some of them show their association with 3–4-cm-wide feeder dikes (Fig. 5; A and B), others lack such features (Fig. 5; C and D). The second group of structures with no feeder dikes also contains clasts, but some of them show downward bending of layers at the margin of the vent (Fig. 5C). One possible explanation is that such deformation features are formed due to layer collapse caused by ground shaking and not necessarily associated with an explosive phase as in typical sandblow formation. The clasts within such types of craters may have been derived from the top clay bed rather than from the sidewalls of a feeder dike. Such features have been characterized as dewatering canals formed under aqueous conditions triggered by ground shaking (Becker et al. 2006).

The minimum ages of the liquefaction features range from AD 1613–1723 to 1814–1854 (Table 2). These OSL dates closely correlate with the earthquake of 1833, which originated in the Nepal Himalaya, and is the only

known event of that interval. Two pieces of wood obtained from two levels of this section were dated at BC 352-AD 132 and AD 988–1116, respectively (Fig. 5; B and C). But these allochthonous materials, as they must have been transported from elsewhere, are not useful in constraining either the depositional age of sedimentary layers or the sandblows.

4 Discussions and conclusions

The deformed sedimentary layers identified in the sections of the northern Bihar and eastern Uttar Pradesh show characteristics of liquefaction triggered by earthquakes distinguishing them from regular sedimentation. These include association with feeder dikes, presence of clasts, and lateral tapering of the sandy layers. Many of these characteristics evident in the 1934 and 1988 liquefaction features are preserved in the upper parts of the local stratigraphy. The characteristics of historically recent sandblows were useful in defining the out-of-sequence beds at deeper levels of the sections. The age constraints of these beds suggest that

they were formed in an episodic fashion and more than seven generations of liquefaction are identified in this study (Fig. 6).

The examples of earthquakes (1934, 1833 and 1988) show that the Bihar Plains are most vulnerable to the seismic activity originating from the Himalaya and also from additional sources under the Nepal *terai* Plains. Although it is important to classify the earthquake sources of the respective liquefaction features, as identified in our study, spatially restricted investigations based on only a few sections are insufficient to successfully interpret individual sizes of the causative earthquakes. But the paleo-earthquake data from the Himalayan foothills offer some benchmark dates for comparison with our results from the plains. These data allow us to correlate the liquefaction episodes dated between AD 829–971, 886–1090 and 907–1181 (contemporaneous dates of liquefaction from sites 1 and 2) to a great earthquake of AD ~1100 from central eastern Nepal (Lavé et al. 2005). If one of these liquefactions is correlative to the great earthquake reported from the trenching on the frontal thrust, then it is reasonable to suggest an elapsed time of ~900 years before the great earthquake of 1934.

Our studies also provide a template for later medieval earthquakes that impacted the region. The liquefaction dated AD 1130–1376 from site 3 points to an earthquake in the twelfth to thirteenth century. Although a Nepal earthquake of AD 1255 is the closest historical event, it is tenuous to suggest a correlation between the two, based on one exposure of a liquefaction layer. Events occurring between AD 1117–1572 and 1492–1672 are

also identified from site 4. The former date has a large uncertainty while the latter is more reliable. Although it is tempting to compare the latter date with the earthquake of 1505, we believe that owing to the distance to the presumed source at the Tibet border with central Nepal, this event is unlikely to have generated liquefaction in the Bihar Plains, where our study sites are located. It is equally possible that the AD 1681 earthquake reported from Nepal, on the basis of historical accounts, may have produced liquefaction in the Bihar Plains, if it was similar to the mechanisms of the 1833 earthquake. Additional paleoliquefaction data need to be gathered from the plains of Uttar Pradesh and Bihar to confirm or refute any of the above generalizations.

The upper most parts of our sections in the Bihar Plains are highly disturbed by plowing activities, but the youngest sandblow cones (emplaced in the 1934 and 1988) are discernible as white sandy patches with rip-up clasts within the recent soil formation (e.g., sites 1 and 2) and the outlines of feeder dikes can be observed (e.g., site 1). The ages obtained from sites 1, 4, and 5 on antecedent liquefactions (AD 1814–1862, 1733–1839, and 1814–1854, respectively) within dating uncertainties imply that the liquefaction due to the 1833 event (probably owing to its location) is more pervasive in the Bihar and eastern Uttar Pradesh Plains than what was summed up dismissively as small-scale ground failures (but no liquefaction) in a few sites in the extant reports of the earthquake (see Bilham 1995). The liquefaction due to the April 25, 2015 Nepal earthquake in the Bihar Plains appears to be more restricted though both events were of similar magnitude.
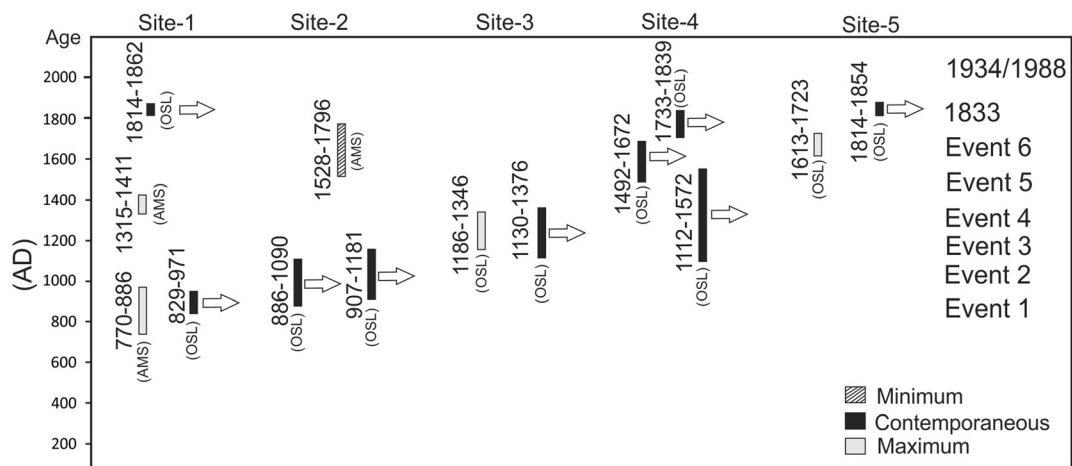

Fig. 6 Space-time diagram showing radiocarbon and luminescence ages obtained from the study sites (vertical dimensions of each box span age limits). *Arrow heads* indicate preferred ages of liquefaction episodes and known dates of medieval earthquakes are given in *brackets*

The Bihar Plains show high liquefaction susceptibility and is a critical area (in the human developmental sense) that is vulnerable to high-intensity shaking from earthquakes sourced in the eastern Nepal Himalaya, exemplified by the great 1934 earthquake as well as by major (e.g., 1833) and strong (e.g., 1988) earthquakes. The present study indicates that this region (including seismic sources in the Himalaya as well as the Nepal Plains) is highly productive in terms of damaging earthquakes. The available data suggest that the combined recurrence interval for moderate to large earthquakes in the Bihar segment could be 124 ± 63 years. This study, as it is restricted to only a few sites, cannot resolve the fundamental questions on the estimates of ground shaking from respective earthquakes or their sizes, nor can it resolve the questions on the distance to the source zones of those earthquakes. As a first attempt in this region, we are only providing a tentative time series of earthquakes that impacted a part of the Gangetic alluvial plains in the last 1500 years that is open to revision in the future. A wider sampling of liquefaction features carried out through a regionally representative investigation may be able to throw further light on questions regarding the source zones of the medieval earthquakes and their corresponding sizes. The present study offers a template for future studies that aims to obtain further confirmatory evidence for the developing an understanding of the recurrence pattern of great earthquakes at the source region of the great 1934 earthquake as well as of more frequent major earthquakes from other sources in eastern central Nepal.

References

Ambraseys N, Jackson D (2003) A note on early earthquakes in northern India and southern Tibet. Cur Sci 84:571–582

Ambraseys N, Douglas J (2004) Magnitude calibration of north Indian earthquakes. Geophys J Int 159:165–206

Becker A, Davenport CA, Eichenberger U, Gilli E, Jeannin PY, Lacave C (2006) Speleoseismology: a critical perspective. Jour Seism 10:371–388

Bilham R (1995) Location and magnitude of the 1833 Nepal earthquake and its relation to the rupture zones of contiguous great Himalayan earthquakes. Cur Sci 69:101–128

Chen W-P, Molnar P (1977) Seismic moments of major earthquakes and the average rate of slip in Central Asia. Jour Geophys Res 82:2945–2969

Dunn JA, Auden JB, Ghosh AMH, Roy SC, Wadia DN (1939) The Bihar-Nepal Earthquake of 1934. Geol Surv India Mem 73, 391p

Ghimire S, Minoru K (2007) Source process of the Ms = 6.6, Udayapur earthquake of Nepal India border and its tectonic implications. Jour Asian Ear Sci 31:128–138

Housner GW (1958) The mechanism of sandblows. Bull Seism Soc Am 48:155–161

Hough S, Bilham R (2008) Site response of the Ganges basin inferred from re-evaluated macroseismic observations from the M 8.1 Shillong 1897, M 7.8 Kangra 1905 and 1934 Nepal M 8.1 earthquakes. Jour Ear Sys Sci 117:773–782

Lavé JD, Yule S, Sapkota K, Bassant C, Madden M, Attal, Pandey R (2005) Evidence for a great medieval earthquake (1100 AD) in the Central Himalayas, Nepal. Science 307:1302–1305

Murray AS, Wintle AG (2000) Luminescence dating of quartz using an improved single-aliquot regenerative-dose protocol. Radiat Meas 32:57–73

Murray AS, Wintle AG (2003) The single-aliquot regenerative dose protocol: potential for improvements in reliability. Radiat Meas 37:377–381

Nandy DR, Choudhury AK, Chakraborty C, Narula PL (1993) Bihar-Nepal earthquake, August 20, 1988. Spec Publ Geol Surv India 31, 104p

Obermeier SF, Gohn GS, Weems RE, Gelinas RL, Rubin M (1985) Geological evidence for recurrent moderate to large earthquakes near Charleston, South Carolina. Science 227:408–411

Obermeier SF (1994) Using liquefaction-induced features for paleoseismic analysis. US Geol Surv Open File Rept 94–663 Chapter A: 1–58.

Obermeier SF, Jacobson RB, Smoot JP, Weems RE, Gohn GS, Monroe JE, Powars DS (1995) Earthquake-induced liquefaction features in the coastal setting of South Carolina and in the fluvial setting of the New Madrid seismic zone. US Geol Surv Prof Paper 1504:44

Parameswaran R, Thulasiraman N, Rajendran K, Rajendran CP, Mullick R, Wood M, Lekhak, H (2015). Seismotectonics of the April-May 2015 Nepal earthquakes: an assessment based on the aftershock patterns, surface effects and deformation characteristics: Asian Jour Ear Sci doi:10.1016/j.jseaes.2015.07.030

Pandey MR, Molnar P (1988) The distribution of intensity of the Bihar-Nepal earthquake of 15 January 1934 and bounds on the extent of the rupture zone. Jour Geol Soc Nepal 5:22–44

Pandey MR, Tandukar RP, Avouac JP, Lavé I, Massot JP (1995) Evidence for recent interseismic strain accumulation on a mid-crustal ramp in the central Himalaya of Nepal. Geophys Res Lett 22:751–758

Rajendran CP, Talwani P (1993) Paleoseismic indicators in Bluffton-Hilton Head area: an appraisal of their tectonic implications. Geology 21:987–990

Rajendran CP, Rajendran K (2001) Characteristics of deformation and past seismicity with the 1819 Kutch earthquake, northwestern India. Bull Seism Soc Am 91:407–426

Rajendran CP, Rajendran K (2005) The status of central seismic gap: a perspective based on the spatial and temporal aspects of the large Himalayan earthquakes. Tectonophysics 395: 19–39

Rajendran CP, Rajendran K, Sanwal J, Sandiford M (2013) Archeological and historical database on the medieval earthquakes of the central Himalaya: ambiguities and inferences. Seism Res Lett 87:1098–1108

Rajendran CP, John B, Rajendran K (2015) Medieval pulse of great earthquakes in the central Himalaya: viewing past activities on the frontal thrust. Jour Geophys Res. doi:10.1002/2014JB011015

Rana BS (2013) The great earthquake in Nepal (first published in Nepali in 1934; translated to English from the 2nd Nepali edition (1935) by Kesar Lall), Ratna Pustak Bhandar, Kathmandu, Nepal, 136p

Reimer PJ, Bard E, Bayliss A, Beck JW, Blackwell PJ, Ramsey CB, Buck C, Cheng H, Edwards RL, Friedrich M, Grootes PM, Guilderson TP, Haflidason H, Hajdas I, Hatté C, Heaton TJ, Hoffmann DL, Hogg AG, Hughen KA, Kaiser KF, Kromer B, Manning SW, Niu M, Reimer RW, Richards DA, Scott EM, Southon JR, Staff RA, Turney CSM, van der Plicht J (2013) IntCal 13 and MARINE13 radiocarbon age calibration curves 0–50000 years calBP. Radiocarbon 55: 1869–1887. doi:10.2458/azu_js_rc.55.16947

Russ DP (1979) Late Holocene faulting and earthquake recurrence in the Reelfoot Lake area, northwestern Tennessee. Geol Soc Am Bull 90:1013–1018

Sapkota SN, Bollinger L, Klinger Y, Tapponnier P, Gaudemer Y, Tiwari D (2013) Primary surface ruptures of the great Himalayan earthquakes in 1934 and 1255. Nat Geosci 6: 71–76, http://dx.doi.org/10.1038/ngeo1669

Saucier RT (1989) Evidence for episodic sandblow activity during the 1811–1812 New Madrid (Missouri) earthquake series. Geology 17:103–106

Seeber L, Armbruster JG (1981) Great detachment earthquakes along the Himalayan arc and long-term forecasting. In: Simpson DW, Richards P (eds) Earthquake prediction—an international review., Maurice Ewing Series, Am Geophys Union 4: 259–277

Seed HB (1979) Soil liquefaction and cyclic mobility for level ground during earthquakes: proc. Jour Geotech Eng 105: 201–255

Sims JD (1973) Earthquake-induced structures in sediments of Van Norman Lake, San Fernando, California. Science 182: 161–163

Sims JD, Garvin CD (1995) Recurrent liquefaction induced by the 1989 Loma Prieta earthquake and 1990 and 1991 aftershocks: implications for paleoseismicity studies. Bull Seism Soc Am 85:51–65

Sukhija BS, Rao MN, Reddy DV, Nagabhushanam P, Kumar D, Lakshmi BV, Sharma P (2002) Palaeoliquefaction evidence of prehistoric large/great earthquakes in north Bihar, India. Cur Sci 83:1019–1025

Talwani P, Cox J (1985) Paleoseismic evidence for recurrence of earthquakes near Charleston. Science 229:379–381

Tuttle MP, Seeber L (1991) Historic and prehistoric earthquake-induced liquefaction in Newbury, Massachusetts. Geology 19:594–597

Tuttle MP, Schweig E III, Campbell J, Thomas PM, Sims JD, Lafferty RH III (2005) Evidence for New Madrid earthquakes in AD 300 and 2350 BC. Seism Res Lett 76:489–501

Tuttle MP, Shukri HA, Mahdi H (2006) Very large earthquakes centered southwest of the New Madrid seismic zone 5,000–7,000 years ago. Seism Res Lett 77:664–678

Youd TL (1973) Liquefaction, flow, and associated ground failure. US Geol Surv Circ 688:1–12

Youd TL (1984) Recurrence of liquefaction at the same site. Proc. 8th World Conf. Earthquake Eng 3:231–238